ARTICLE Communicated by Carl van Vreeswijk

Dynamical Consequences of Fast-Rising, Slow-Decaying Synapses in Neuronal Networks

Bard Ermentrout
bard@math.pitt.edu
Department of Mathematics, University of Pittsburgh, Pittsburgh, PA 15260, U.S.A.

Synapses that rise quickly but have long persistence are shown to have certain computational advantages. They have some unique mathematical properties as well and in some instances can make neurons behave as if they are weakly coupled oscillators. This property allows us to determine their synchronization properties. Furthermore, slowly decaying synapses allow recurrent networks to maintain excitation in the absence of inputs, whereas faster decaying synapses do not. There is an interaction between the synaptic strength and the persistence that allows recurrent networks to fire at low rates if the synapses are sufficiently slow. Waves and localized structures are constructed in spatially extended networks with slowly decaying synapses.

1 Introduction

There has been a great deal of recent interest in the mechanisms that underlie persistent activity in the cortex during various cognitive tasks (Camperi & Wang, 1998; Lisman, Fellous, & Wang, 1998; Wang, 1999, 2001; Compte, Brunel, Goldman-Rakic, & Wang, 2000; Gutkin, Laing, Colby, Chow, & Ermentrout, 2001; Laing & Chow, 2001; Rubin, Terman, & Chow, 2001). The most notable of these are delayed-response experiments (Fuster, 1973; Goldman-Rakic, 1987). In these tasks, an animal fixates on a point in its visual field. Another spot, peripheral to the fixated spot, comes on briefly. The second spot is removed, and the animal must maintain its current gaze until a third signal is given. The animal then makes a saccade (eye movement) to the point of the second spot and is rewarded. During this task, the animal must "remember" the location of the peripheral spot for up to several seconds after it disappears. Recordings in cortex have revealed that neurons whose receptive fields are in the area of the second spot continue to fire after the stimulus is removed. Thus, many people have asserted that this activity is a consequence of spatially localized persistent activity. However, since it is difficult to record from many points simultaneously, the experimental evidence for this mechanism is circumstantial.

Persistent activity is more readily found in cortical slice preparations (Sanchez-Vives & McCormick, 2000) in which various pharmocological

agents have been applied, such as blockers of inhibition. This activity typically takes the form of slowly moving wave (Wu, Guan, & Tsau, 1999; Wu & Guan, 1999) but has been cited as being a possible direct physiological correlate of persistent activity seen in vivo (Sanchez-Vives & McCormick, 2000).

Nonlinear recurrent neural networks have many computational advantages over simple feedforward systems. This is because the recurrent connections allow the network to maintain many different stable states. The nonlinearity in these simple models is manifested by their ability to switch between a high and low state of "firing." There are several ways in which a network can become bistable. It can be an intrinsic property of neurons comprising the network (such as in the two-compartment models of Booth & Rinzel, 1995), or bistability can arise from recurrent network properties properties. Since "neural network" models are more representative of networks of cells where the detailed properties of the membranes are averaged out, in this article, we will consider the role of recurrent synaptic excitation in creating bistability in networks. Bistability and recurrent excitation have been implicated in many aspects of cortical physiology. For example, epileptic activity is thought to be maintained by the strong recurrent excitation between neurons (Traub & Miles, 1991). In disinhibited cortical slices, recurrent excitation is responsible for the propagation of synaptically generated bursts (Golomb & Amitai, 1997). Delayed-response tasks as well as localized attractors have been modeled via neural nets by recurrent excitatory interactions between model cells (Amari, 1977; Lisman et al., 1998; Compte et al., 2000; Laing & Chow, 2001; Gutkin et al., 2001; Wang, 1999, 2001) Indeed, Lisman et al. (1998) use the nonlinear voltage dependence of the NMDA synapse to construct a bistable neuron model. Here, we will consider a simpler scenario, where just the slowness of the excitatory decay leads to the bistability in a recurrent network.

There has been a large amount of theoretical analysis of the delayed-response task using neural network or firing-rate models. The earliest models were those of Amari (1977), who analyzed a neural network with lateral inhibition and self-excitation,

$$u_t(x,t) = -u(x,t) + \int_{-\infty}^{\infty} w(x-y)F(u(y,t))\,dy, \tag{1.1}$$

where $u(x,t)$ is the activity of a neuron at spatial point x and $w(x)$ is a weight function that is similar to a difference of gaussians. The nonlinear function $F(u)$ is a step function in Amari's original analysis and in a later paper (Kishimoto & Amari, 1979) is allowed to be smooth. Amari shows that networks such as this exhibit a localized region of maintained activity (which we call a *bump*); furthermore, formal stability is also proven. More recently, we (Pinto & Ermentrout, 2001a) examined multilayer models of this type in which the excitation and inhibition are separated into two populations.

Camperi and Wang (1998) analyze a similar network, but the individual units are themselves bistable. They claim that this stabilizes the bump to noise. The evidence for bistability in individual neurons is not clear, but one can circumvent this assumption by assuming that there are strong self-connections in the network. In a more recent article and one that is more directly related to this study, Wang (1999, 2001) studied the roles of recurrent excitation, NMDA synapses, and negative feedback via spike frequency adaptation on the existence of persistent states in a network. Compte et al. (2000) and Laing and Chow (2001) studied spatially localized activity in a network of spiking neurons. Laing and Chow showed the necessity of maintaining an asynchronous state within the localized bump and demonstrated the loss of stability to traveling waves. Both Gutkin et al. (2001) and Laing and Chow (2001) showed that synchronizing the neurons leads to the destruction of the localized activity. Recently, Netoff and Schiff (2002) showed a similar effect in experimentally induced epilepsy.

Excitatory connections between cortical neurons are mediated by the neurotransmitter glutamate. Two important classes of receptors are the AMPA and NMDA receptors. When glutamate binds to AMPA receptors, there is a brief depolarization of the neuron (that is, the potential is increased), which decays within a few milliseconds. The rise time of AMPA-mediated synapses is almost instantaneous. In contrast, NMDA receptors are more complicated. In normal conditions, the receptors do not open unless the neuron is already depolarized. However, it is possible to remove the voltage dependence of the receptor by bathing the neurons in a medium with a low concentration of magnesium. NMDA receptors rise rather quickly but decay at a much slower rate—anywhere from 50 to 150 milliseconds. This is the type of synapse that we will study in this article.

There have been several studies of neuronal models and networks with slow synapses. In these articles, both the rise time and the decay time of the synapses are slow. That is, the synapses obey equations of the form

$$\frac{ds}{dt} = \epsilon F(s, v),$$

where v is the membrane potential of a neuron associated with the synapse. This enables one to apply the method of averaging when the potential, $v(t)$, is a periodic function. Frankel and Kiemel (1993) were the first to study this when coupling between neurons is weak. (We discuss their results in detail in section 3.) Bressloff and Coombes (2000) analyzed phase instabilities in coupled integrate-and-fire neurons brought on when the synapses become sufficiently slow. In Ermentrout (1994), we studied spatially organized networks of neurons with slow synapses and showed how one could obtain simpler neural network models by applying formal averaging. The synaptic dynamics in this article are governed by equations of the form

$$\frac{ds}{dt} = a(v)(1 - s) - \epsilon s.$$

Only the decay is slow, so that the resulting dynamics are a cartoon for the mechanism of NMDA receptors.

This article is divided as follows. In section 2, we characterize the requirements for a synaptically coupled network to be bistable. That is, we will assume that the neurons are excitable and that the coupling between them is what enables a maintained activity state. We assume that the individual neuron models are channel based and that the synapses obey simple first-order dynamics. We will first give a detailed geometric analysis of a single self-coupled neuron. Next, we numerically examine globally connected networks of synaptically coupled neurons. We also analyze the minimum firing rate possible in these networks as a function of the number of neurons and the decay rate of the synapse. In particular, we show that the firing rate of the recurrent network can be arbitrarily low if we use sufficiently slow synapses. In section 3, we assume that the synapses decay slowly, an assumption that is required based on results of section 2. We show that this reduces a pair of coupled neurons to a simple phase model of two weakly coupled oscillators. We show that the synchronous state is unstable and the neurons tend to oscillate asynchronously. We contrast this to synapses that both rise and decay slowly. Finally, we show how a spatially organized network of neurons with slowly decaying synapses can be formally reduced to networks with piecewise constant nonlinearities for which we can apply the classical Amari analysis.

2 How a Network Becomes Bistable

In this section, we geometrically describe how recurrent excitatory synapses lead to bistability in a neuron. Wang (1999) has extensively analyzed this question using an integrate-and-fire model and a self-consistent theory. We will discuss his results in the light of our own analysis later in this section.

To motivate the analysis in this section, we first look at a single self-coupled neural network model:

$$u_t = -u + f(u + I). \tag{2.1}$$

As usual, $f(u)$ is a nonlinear monotone increasing function. Here, u represents the firing rate of the neuron. If the nonlinearity is sufficiently sharp, then for a range of values of the input, I, the model is bistable. That is, there are two stable fixed points—one low and the other high. In many models, $f(u)$ is defined to be piecewise continuous and vanishes identically if the argument is below a threshold. This means that if the input is small, the unit does not fire, and as the input increases, the neuron fires at some finite rate. For continuous functions f, there is in addition to the two stable fixed points an unstable fixed point. As the input decreases, the unstable fixed point merges with the stable nonzero firing rate and disappears. Let us interpret this from the point of view of a spiking neuron that has a self-synapse.

The zero state of equation 2.1 corresponds to the neuron sitting at rest with insufficient input to cause it to fire. The stable nonzero state corresponds to the neuron firing at a fixed nonzero frequency, that is, a stable periodic orbit for the spiking system. The unstable fixed point thus corresponds to an unstable periodic orbit of the spiking neuron. This state will never be experimentally observed. However, as the input to the neuron is decreased, the stable and unstable periodic orbits will merge and disappear.

Consider next a pair of mutually excitatorily coupled neurons:

$$\begin{aligned} u_{1t} &= -u_1 + f(u_2 + I) \\ u_{2t} &= -u_2 + f(u_1 + I). \end{aligned} \tag{2.2}$$

This system can be readily analyzed in the phase plane; the only equilibria are those in which $u_1 = u_2$. As in the scalar case, as the common input changes, these fixed points appear or disappear symmetrically. There is essentially no difference in the global behavior between equations 2.1 and 2.2. Let us now look at the same situation with a spiking model such as a pair of coupled Hodgkin-Huxley (HH) type models. If the synapses decay slowly enough and the coupling between the two cells is excitatory and sufficiently strong, then the reciprocal interactions enable both cells to fire repetitively. (We assume there are no slow processes that act to hyperpolarize the neurons and stop the persistent firing, as in van Vreeswijk & Hansel, 2001.) Thus, the stable active state corresponds to both neurons firing at the same firing rate. However, there is no information about phase conveyed by the neural network models equation 2.2, while in the HH models, the relative phases of the spiking could be any of an infinite number of possibilities. These considerations lead us to ask several questions about self-coupled and network-induced bistability in HH models. For a scalar network (firing-rate) model with self-coupling, loss of bistability is through a saddle node of equilibria. But these nonzero equilibria correspond to periodic firing of the neuron so that the loss of bistability is equivalent to the merging of an unstable and a stable periodic orbit. However, firing-rate models do not make it clear how the periodic orbits arise in the HH-type models. Thus, we ask how a single self-coupled HH neuron can maintain persistent activity; that is, how does repetitive firing arise?

2.1 The Dynamics of a Single Self-Coupled Neuron. There are infinitely many possible models for neurons in which one could analyze the behavior of self-coupling. Rather than attempt this hopeless task, we instead take a different approach. We will assume a certain class of neural models and then use a canonical reduction of these models and analyze that system. We will then use numerical bifurcation methods to show that full-fledged models behave the same as the canonical model. The systems of interest

have the following form:

$$C\frac{dV}{dt} = I - \sum_k g_k(t)(V - E_k) - g_{syn}s(V - E_{syn}) \tag{2.3}$$

$$\frac{dz_k}{dt} = F(z_k, V)$$

$$\frac{ds}{dt} = a_s(V)(1 - s) - s/\tau \tag{2.4}$$

Here, $g_k(t)$ is a nonlinear conductance gated by the variable(s) z_k, I is an applied current, $g_{syn}s$ is the self-synaptic conductance, $a_s(V)$ is the rate at which the synapse is turned on, and τ is the synaptic time constant. The synapse, equation 2.4, is typical of the models that are used in the analysis and simulation of neural models (Destexhe, Mainen, & Sejnowski, 1994). We will assume that in the absence of external input and in the absence of the synapse that the neuron has a stable resting state, and this is the only steady solution. Suppose that there is no synapse and suppose that as the applied current, I, is increased, the neuron begins to fire repetitively. There are several ways in which a neuron can begin to fire rhythmically. We will assume that the onset of repetitive firing is through a saddle node on a limit cycle (see Figure 1). This type of spiking behavior is called type I and has been the subject of numerous theoretical articles (Ermentrout & Kopell, 1986; Ermentrout, 1996; Izhikevich, 1999; Rinzel & Ermentrout, 1998). Many models of cortical neurons have this property (in contrast to the HH squid axon model, type II, for which the onset of repetitive firing is through a subcritical Hopf bifurcation.)

The main difference between type II and type I firing is that in the latter, the frequency of firing can be arbitrarily low. This is crucial in cortex, since it leads to a very broad gain function. There are also other important

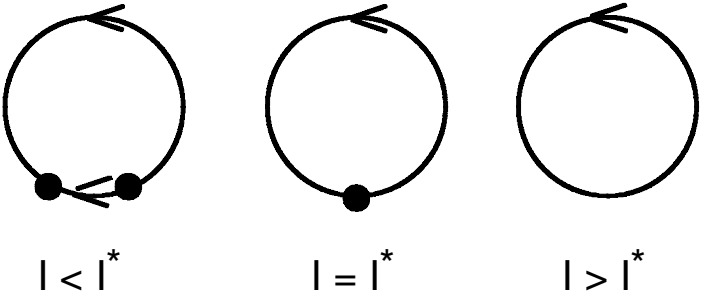

Figure 1: Bifurcation from a stable rest point to a stable limit cycle as the current I is increased. Below I^* is a closed circle containing two fixed points. These merge and disappear, leaving the closed circle representing repetitive firing.

computational consequences of this type of firing (Ermentrout, 1998a; Ermentrout, Pascal, & Gutkin, 2001). Given that we have type I firing, we can now ask what happens with a single self-synaptic connection. If the neuron is at rest, then the synapse will have no effect. However, if we inject a brief depolarizing current that causes the neuron to fire, then the synaptic current may be enough to sustain the neuron in a repetitively firing state. There are two conditions that are necessary to maintain repetitive firing: (1) the conductance must be sufficiently large, and (2) the synapse must persist longer than the refractory period of the neuron. If these two conditions are met, then it is possible to reexcite the neuron and thus produce a repetitively spiking neuron. (Here, we ignore such effects as adaptation and synaptic fatigue, which may cause the neuron to cease firing eventually.) A strong enough hyperpolarizing input will stop the firing; the self-synapse has led to a "bistable" switch. Although the neuron has no intrinsic currents that make it bistable, the self-synapse is enough to induce this bistability. We now attempt to determine the dynamics that underlie this bistability.

The key to understanding the conditions for synaptic bistability is to consider a simplified model that has all of the properties of a type I neuron but can be easily analyzed. Ermentrout and Kopell (1986) and Hoppensteadt and Izhikevich (1997) have shown that near the bifurcation, all type I membranes are equivalent to a simple one-dimensional model on the circle

$$\theta' = 1 - \cos\theta + (1 + \cos\theta)R(t), \tag{2.5}$$

where $R(t)$ represents all the inputs to the neuron and θ describes the phase around the circle depicted in Figure 1. Note that when R is a negative constant, then there are two fixed points for equation 2.5 while for R positive, there are none and θ increases monotonically around the circle representing the periodic solution. It is a simple procedure to add a "synapse" to this reduced model. Firing takes place when θ crosses π. Thus, we let

$$R(t) = I + gs \tag{2.6}$$

$$s' = K(\theta)(1 - s) - s/\tau \tag{2.7}$$

$$K(\theta) = \alpha \exp[-\beta(1 + \cos\theta)]. \tag{2.8}$$

The input, R, to the neuron consists of a constant bias I and a "synaptic input." (Note that the dimensions of g are not conductance since the reduced model no longer has physical units associated with it; however, the synaptic input appears in the reduction in this manner (see Ermentrout, 1998a).) The synapse obeys the same dynamics as equation 2.7, with the exception that the rate at which the synapse is turned on depends on θ rather than the voltage V. If β is large, then the function K is close to zero except for θ near π, when it peaks to α. We now have a two-dimensional system on the cylinder $S \times R$ and can use phase-plane methods to analyze the onset of bistability in the self-coupled system.

We assume $I < 0$, since there must be a stable resting state in the absence of the synaptic activation. Since the synapse has essentially no effect on the model unless the neuron is firing, the equilibria for this model are those of equation 2.5, when $g = 0$. Thus, there are two fixed points given by $(\theta^{\pm}, 0)$ where

$$\theta^{\pm} = \pm \arccos \frac{1+I}{1-I}.$$

The positive fixed point is a saddle point, and the negative one is a stable node. The stable manifold of the saddle point is nearly tangent to the line $\theta = \theta^{+}$, while the unstable manifold is tangent to the line $s = 0$. The way to understand the transition to a bistable system is to study the stable and unstable manifolds of this saddle point as the conductance is varied. In Figure 2, I sketch the conjectured global behavior of the system in equations 2.5 and 2.7 as the "conductance" g is decreased. For strong enough conductances, the system has a stable periodic solution and a stable fixed point. The stable manifold of the saddle point acts as a separatrix between the two behaviors; for small perturbations from the resting state, the solution decays to rest. For perturbations that take θ past the saddle point (i.e., cross threshold), the model sustains repetitive activity. The loss of bistability takes place through the series of bifurcations shown in the figure. The stable and unstable manifolds of the saddle point merge to form a homoclinic. This leads to an unstable periodic solution, which collides with the stable periodic orbit and annihilates it, leaving only the stable rest state. A similar sequence occurs if instead of the conductance, the time constant of the synapse is changed from a larger (longer-lasting synapses) to a smaller (faster synapses) value.

Recalling the neural net model, equation 2.1, the bistability was lost when the unstable fixed point coalesced with the stable fixed point. Since the nonzero fixed points of the neural network model correspond to periodic orbits (they represent a firing rate), the loss of bistability through a fold bifurcation is analogous. However, the formation of the unstable limit cycle is never clearly delineated in the neural network system. Here, we see that it is quite subtle.

Obviously, the sequence above may not be relevant to a full conductance-based model. We have numerically analyzed a model that incorporates fast spiking channels (see the appendix for the model used in the simulations) and find the same sequence of behavior. The conditions for this to occur are straightforward. Suppose that the decay of the synapse is the slowest timescale in the model equations. The saddle point has a one-dimensional unstable manifold and an $(n-1)$-dimensional stable manifold. The return to the stable manifold will be dominated by the slowest rate, which in this case is the synapse. Thus, we can essentially reduce the high-dimensional system to a two-dimensional system, as we considered. Finally, the unstable manifold leaves the saddle point at a rate $\lambda_u > 0$, and the slowest rate of the stable manifold is approximately $\lambda_s = -1/\tau$. Since τ is large, this means that

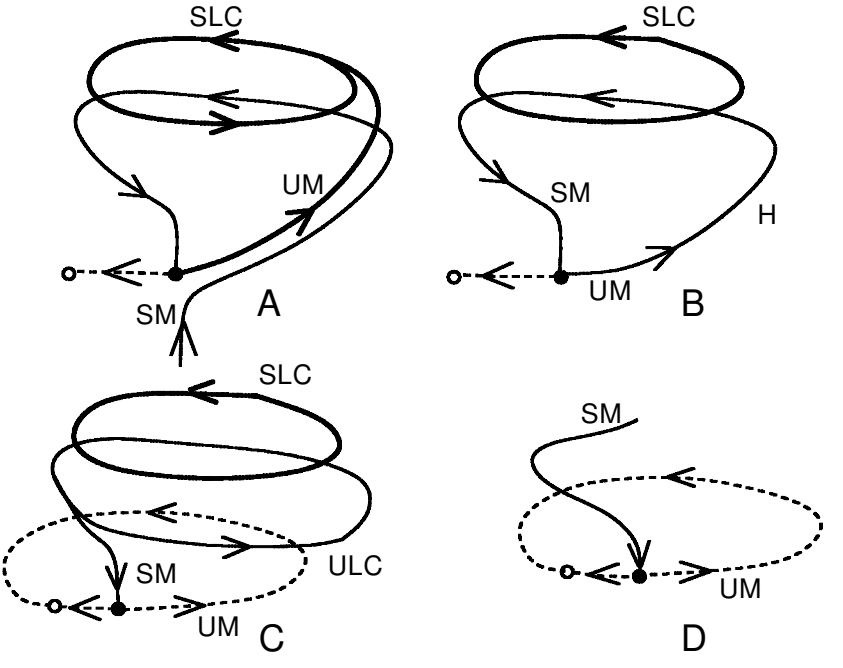

Figure 2: Bifurcation as the conductance is decreased. (A) There is a stable limit cycle (SLC), and the unstable manifold (UM) of the saddle point wraps around it. The stable manifold (SM) is close by. (B) The stable and unstable manifolds of the saddle point coalesce, leaving an unstable homoclinic orbit (H). (C) The homoclinic is broken into an unstable limit cycle (ULC). (D) The stable and unstable limit cycles merge and disappear for low conductance.

$\lambda_u + \lambda_s > 0$, which implies that the periodic solution bifurcating from the homoclinic is unstable. Geometrically, this is why we need the time constant of the synapse to be large.

This description, along with the two-dimensional analysis shown in Figure 2, imply that the limiting factors in determining whether the neuron can maintain an active state are the size of the synaptic conductance and the time constant of the synapse. We expect an inverse relationship: the larger is τ, the smaller that g_{syn} can be. Since the minimum value of the synaptic strength for a given value of the time constant occurs when the stable and unstable periodic solutions merge, it is a simple matter to determine this boundary numerically. Figure 3 shows this curve computed for the biophysical model defined in the appendix. We later show that there is a minimal g_{syn} below which it is impossible to maintain repetitive firing; thus, there is a vertical asymptote for this curve. Because the rate at which the synapse

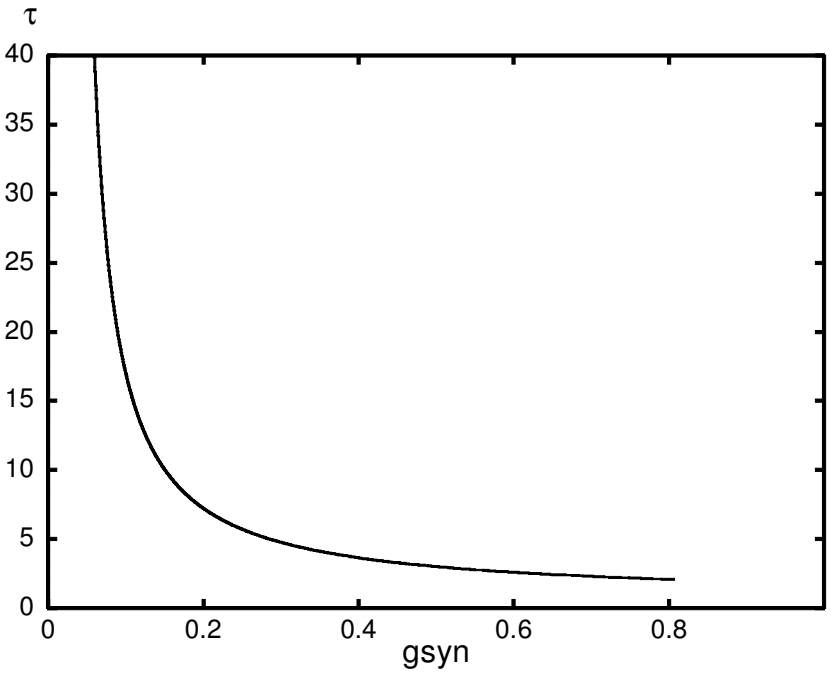

Figure 3: The boundary separating sustained from transient activity. If $(\tau\ g_{syn})$ is above the curve, the neuron is capable of self-sustained activity.

rises is finite, we expect that as $g_{syn} \to \infty$, $\tau(g_{syn})$ will tend to a nonzero limit.

The ideas laid out in the previous paragraphs are for a single self-coupled neuron. A more difficult question arises if we consider a network of neurons instead. The self-coupled case is relevant only if all of the neurons synchronize. However, as we show below, in general, we do not expect neurons to synchronize. Thus, we can ask what is different about the "out-of-phase" case. It turns out that other than quantitative details, there is no difference between the two cases. That is, there is a curve that looks almost identical to Figure 3 for a reciprocally coupled pair of neurons oscillating in antiphase. However, the curve is shifted to the left. That is, for a given τ, the minimal g_{syn} for which persistent behavior exists is smaller than that of the self-coupled (synchronous) model.

If the neuron contains another slow process, such as a spike-frequency adaptation current, then the restriction to two dimensions is not generally correct. If we add adaptation to the conductance-based model, the picture is more complicated; bursting and other behavior are possible (van Vreeswijk & Hansel, 2001). Wang (1999) has studied these cases in a model integrate-

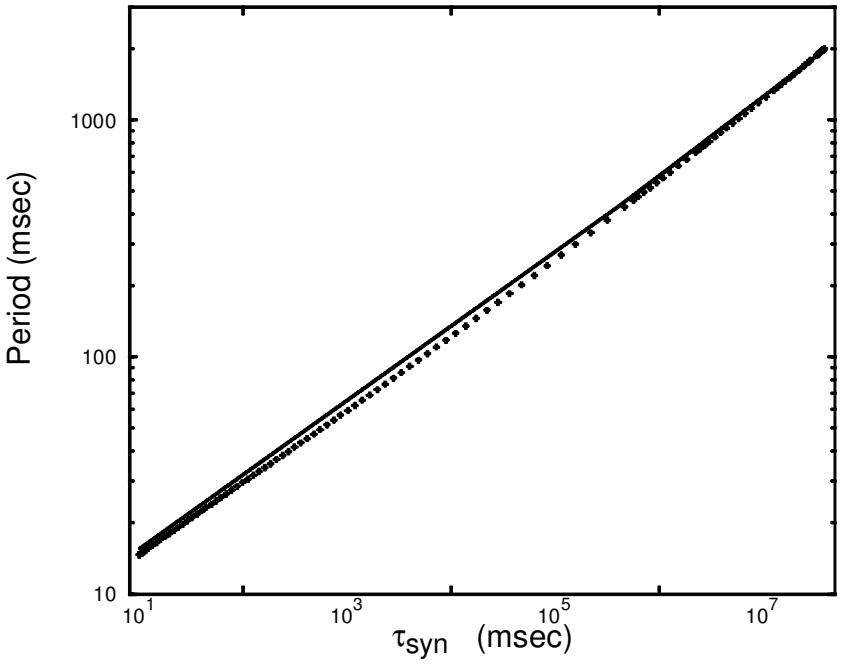

Figure 4: The minimum period of sustained activity as a function of the synaptic time constant for a self-excited conductance-based model. The solid curve is an asymptotic approximation valid for large τ_{syn}. The leading term is $\tau^{1/3}$.

and-fire network in which there is both inhibition and possibly adaptation. One of the main issues that he and others are interested in is maintaining low firing rates in the presence of recurrent excitation. The minimum firing rate that can be sustained by the system occurs at the saddle-node bifurcation, where the unstable and stable periodic solutions merge. Thus, it is of interest to plot this minimum period. In Figure 4, we show the plot of the minimum period as a function of the synaptic time constant for the model (with no adaptation) described in the appendix. On a log-log plot, this is close to a straight line with a slope of one-third.

2.1.1 An Asymptotic Approximation. To understand the scaling of the period with the time constant, we employ a self-consistent theory in the same manner as Wang (1999). The synapse satisfies the equation

$$s' = aq(V)(1 - s) - s/\tau_{syn},$$

where q is the voltage-dependent gate for the synapse. If the firing rate is fast compared to the time constant of the synapse, τ_{syn}, then we can average

this in the manner of Ermentrout (1998a), obtaining

$$s' = af(1-s) - s/\tau_{syn}, \tag{2.9}$$

where f is the firing rate of the neuron. The key point is that the firing rate depends on the strength of the conductance, g, and the bias current, I. Up to rescaling, we can write

$$f = F(I + gs),$$

where F is essentially the firing rate versus current (FI) curve. Thus, at equilibrium, the gating average of the synaptic gating variable satisfies

$$0 = aF(I + gs)(1-s) - s/\tau_{syn}. \tag{2.10}$$

We proceed generally, making no assumptions on the FI curve other than that it vanishes at some critical value of the current (say, $F(0) = 0$) and $F'(I)$ exists for $I > 0$ and is positive. This means that $F(I)$ invertible for $I \geq 0$. Let $F_{inv}(f)$ be the inverse of the FI curve. We remark that $F_{inv}(0) = 0$ and $F'_{inv}(f) > 0$ for $f > 0$. We also require that

$$\lim_{f \to 0} \; fF'_{inv}(f) = 0.$$

(Note that for reasonably behaved functions, $F_{inv}(f)$ satisfying $F_{inv}(0) = 0$ and $F'_{inv}(f) > 0$, this last property holds automatically.) We now show that the minimum firing rate possible, f, in a self-coupled neuron with FI curve $F(I)$, satisfies

$$f^2 F'_{inv}(f) a\tau_{syn} + fF'_{inv}(f) - F_{inv}(f) = -I, \tag{2.11}$$

where $I < 0$ is the applied bias. At equilibrium, we have $f = F(I + gs)$ and $af(1-s) - s/\tau_{syn} = 0$. Combining these two equations, we must solve

$$N(f,g) \equiv a\tau_{syn} f \left(1 - \frac{F_{inv}(f) - I}{g}\right) - \frac{F_{inv}(f) - I}{g} = 0.$$

Recall that the minimum frequency occurs at the value of g for which there is a saddle-node point; that is, $\partial N(f,g)/\partial f = 0$. Differentiating N with respect to f and solving for g gives the critical value of g:

$$g_{\min} = \frac{a\tau_{syn}}{F'_{inv}(f)} + F_{inv}(f) - I + fF'_{inv}(f).$$

We substitute this into the equation $N(f, g_{\min}) = 0$ and after rearranging, we obtain equation 2.11. We are interested in what happens as $\tau_{syn} \to \infty$. As $\tau_{syn} \to \infty$, this can be solved only if $f \to 0$; since $fF'_{inv}(f) \to 0$, we obtain

$$f^2 F'_{inv}(f) \sim \frac{-I}{a\tau_{syn}}. \tag{2.12}$$

Before looking at several examples, we examine the validity of averaging to obtain equation 2.9. Averaging is valid only if the firing rate is considerably larger than $1\tau_{syn}$. This means that $f\tau_{syn} \gg 1$. Equation 2.12 implies

$$fa\tau_{syn} \sim \frac{-I}{fF'_{inv}(f)},$$

and since the denominator of the right-hand side tends to zero, we conclude that $f\tau_{syn} \gg 1$, as required.

As a first example, suppose that near the origin, $F(I) = (CI)^p$ for C, p positive. Then $F_{inv}(f) = f^{1/p}/C$, so that $F'_{inv}(f) = f^{-1+1/p}/(pC)$, and asymptotically, we find

$$f \sim \left(\frac{-pCI}{a\tau_{syn}}\right)^{\frac{p}{p+1}} \tag{2.13}$$

as $\tau_{syn} \to \infty$. In particular, for type I excitable systems, $p = 1/2$, and so the minimum frequency scales as $\tau^{-1/3}$, as we observed. In fact, for the particular case of a square root FI curve, equation 2.11 becomes the cubic equation,

$$a\tau_{syn}f^3 + f^2/2 = -IC/2,$$

from which we obtain

$$f = \left(\frac{-IC}{2a\tau_{syn}}\right)^{\frac{1}{3}} - \frac{1}{6a\tau_{syn}} + O((a\tau_{syn})^{-\frac{5}{3}}.$$

As a second example, suppose that the FI curve is that of the leaky integrate-and-fire model:

$$f = F(I) = (\tau_m \log([I + I_0]/I))^{-1}.$$

Then $F_{inv}(f) = I_0[\exp[1/(\tau_m f)]]^{-1}$ and

$$f \sim \left[\tau_m \log\left(\frac{a\tau_{syn}I_0}{-\tau_m I}\right)\right]^{-1}.$$

Remarks.

1. We note that this averaging approximation gets better if there are many neurons coupled together in an all-to-all fashion, which oscillate asynchronously since they are then all subjected to the same nearly constant synaptic current (see for example, Golomb & Rinzel, 1993; Hansel & Mato, 2001). Hansel and Mato (2001) rigorously show that the firing rate of a large population of excitatory neurons that are firing asynchronously satisfies an equation similar to 2.10. They also demonstrate that when there are inhibitory neurons, it is possible to get low firing rates if there is sufficient inhibitory-inhibitory coupling.

2. Saturation of synapses is necessary for the minimum rate to depend on the decay constant. To see this, we repeat the asymptotic expansion for the analogue of equation 2.10, but without saturation,

$$0 = aF(I + gs) - s/\tau_{syn},$$

from which we find that the critical value of g is

$$g_{\min} = \frac{F'_{inv}(f)}{a\tau_{syn}}$$

so that

$$fF'_{inv}(f) - F_{inv}(f) = -I.$$

The minimal firing rate is dictated by how far away the resting neuron is from the threshold and is independent of the time constants for the synapse. For example, for type I neurons, $f_{\min} = C\sqrt{-I}$.

3. We provide one more approximation to the solution to equation 2.10. If τ_{syn}^{-1} is small, then s is approximately 1 and the firing rate of the neuron is $F(I + g)$ as a function of g. For a type I neuron, we expect the firing rate to be close to a square root of the current past threshold. Thus, $F \approx F_0\sqrt{g - g_0}$ where F_0, g_0 are model-dependent parameters. From this, we obtain a simple approximation of the steady-state average of the synapse, $\bar{s}$, which solves equation 2.10:

$$\bar{s} \approx \frac{aF_0\sqrt{g - g_0}}{aF_0\sqrt{g - g_0} + 1/\tau_{syn}}. \tag{2.14}$$

In Figure 5, we plot this approximation for the self-coupled ionic model described in the appendix. For this model with $\tau_{syn} = 20$, $aF_0 = 0.6$ and $g_0 = 0.032$. The approximation is very good; the range of frequencies is from 25 Hz to 400 Hz.

Summarizing, if the synaptic strength is large enough and the synapse is slow enough, there can be bistability. The transition from bistability to monostability is marked by the collision of an unstable periodic orbit, with the stable periodic orbit representing the sustained firing state. The minimum frequency of the sustained activity occurs at the saddle-node point of the oscillators and scales as the one-third power of the time constant of the synapse. A simple approximation for the averaged synaptic gating variable can be easily obtained.

2.2 Phase Relations in a Coupled System. If we now consider a pair of mutually coupled neurons in analogy to equation 2.2, then we can ask a similar question: What is the mechanism for bistability, and what are the constraints on the coupling strength and the synaptic time course? For example, if both neurons are firing, then they could fire synchronously or

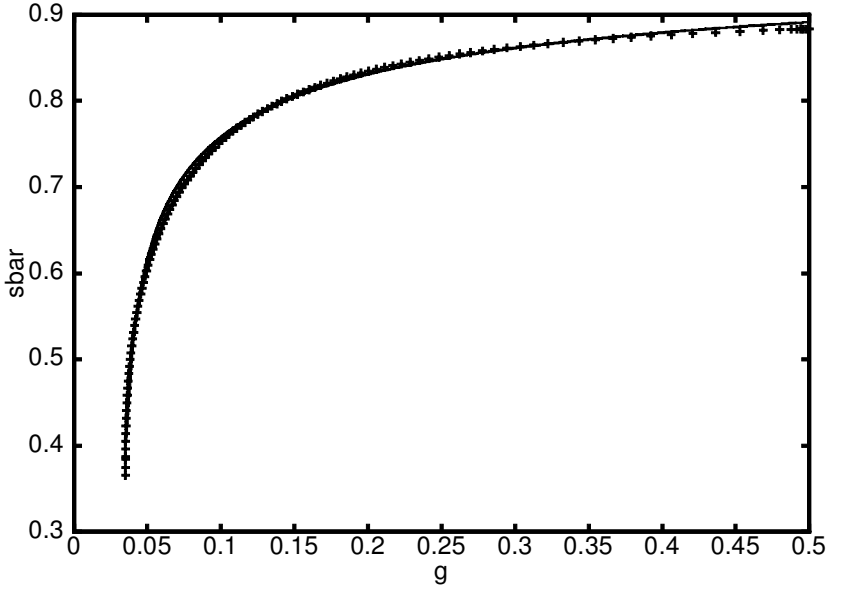

Figure 5: Numerically computed mean value, $\bar{s}$, of the synaptic gating variable for the Traub model described in the appendix as a function of the strength of the self-coupling, g. The solid line is the approximation given by equation 2.14.

out of phase with each other. If they fire synchronously, then the analysis in section 2.1 holds, and there is no difference between this and a single self-coupled neuron. However, if they fire out of phase with each other, then the above analysis does not hold, although, as we discussed, there is little qualitative difference in the existence of bistability.

We show three things in this section. First, a pair of mutually coupled neurons with slowly decaying synapses is shown to behave like a pair of weakly coupled oscillators. Second, we show that in general, the synchronous state is unstable. Finally, we contrast the behavior of the slowly decaying synapses with that of synapses that both rise and decay slowly.

Consider the following general model of a single cell with synaptic inputs:

$$C\frac{dV}{dt} = -I_{ionic}(V, \ldots) - g_{syn}(V - V_{syn}). \tag{2.15}$$

We regard g_{syn} as a constant parameter for the moment. The dots in the function I_{ionic} represent all the other variables and gates that are responsible for the intrinsic propeties of the cell. We can now lay out our assumptions. We assume that for g_{syn} below some critical value, G^*, equation 2.15, has

a single asymptotically stable equilibrium point, and this is the only stable behavior. We assume that at $g_{syn} = G^*$, there is a saddle-node bifurcation to a periodic solution so that for $g_{syn} > G^*$, there is a stable branch of large-amplitude periodic solutions that bifurcate from the saddle node at arbitrary low frequency. This assumption was used in the previous section and holds for a wide class of conductance-based neurons. Recall that these are called type I neurons. Neurons that have type I spiking behavior have an important property: their phase-response curve (the change in phase due to transient perturbations) is nonnegative (Hansel, Mato, & Meunier, 1995; Ermentrout, 1996). Later in this section, we exploit this property.

Now let us consider a model synapse that has a slow decay. For mathematical purposes, we will treat the decay of the synapse as a small parameter, and then we can use asymptotics to understand the bistable nature between two coupled neurons and the phase relationship between their spikes. Consider the model synapse,

$$\frac{ds}{dt} = K(V)(1-s) - \epsilon s, \tag{2.16}$$

where ϵ is a small, positive parameter. The function $K(V)$ vanishes when the neuron is below some threshold and is bounded otherwise. For example, $K(V) = a[\tanh(b(V - V_T))]^+$, where $[x]^+$ means the positive part of x. What happens once V crosses threshold? Then s is incremented by some amount. If the neuron continues to fire, then s reaches 1, and since ϵ is small, s will decay by only a very small amount. Indeed, if the firing rate of the neuron exceeds $1/\epsilon$, then s will be within ϵ of 1 during each cycle of firing. We now couple two identical neurons with this type of synapse:

$$C\frac{dV_i}{dt} = -I_{ion}(V_i, \ldots) - g_{syn}s_j(V_i - V_{syn})$$
$$\frac{ds_i}{dt} = K(V_i)(1-s_i) - \epsilon s_i.$$

We assume that g_{syn} is large enough so that when $s_j = 1$, the neuron fires at a rate large compared to ϵ. Figure 6A shows the result of coupling two biophysical models with such synapses. The neurons oscillate out of phase; synchrony is unstable. $s_i \approx 1$ so that the coupled pair will keep each other on, and we have achieved bistability. Let us look at the phase relationships. Since s_i is close to but less than 1, we can write

$$s_i = 1 - \epsilon S_i.$$

Then

$$\frac{dS_i}{dt} = 1 - K(V_i)S_i + O(\epsilon)$$

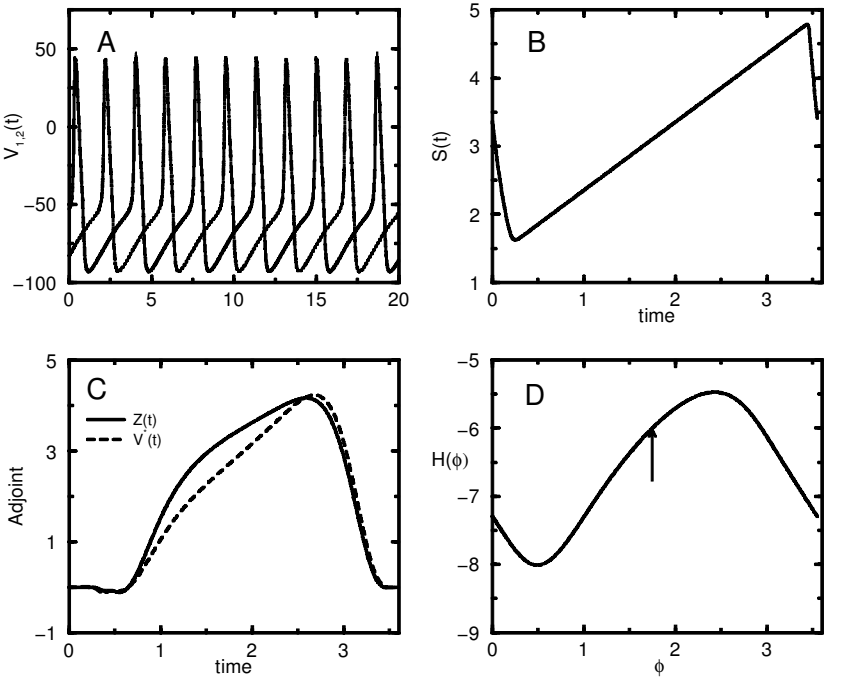

Figure 6: Coupling between two excitatory neurons with slow decay. The model is as in the appendix, with $g_{syn} = 0.25$ and $\tau_{syn} = 50$ ($\epsilon = 0.02$). (A) The potentials of the two coupled neurons showing stable antiphase locking. (B) The rescaled synaptic variable $\hat{S}(t)$. (C) The adjoint, V^* and the quantity, $Z(t) = V^*(t)(V_{syn} - V(t))$. The peak of the voltage occurs at $t = 0$, and the adjoint has been scaled so that the magnitudes match.) (D) The interaction function for slow coupling. The arrow shows $H(T/2)$.

and

$$C\frac{dV_i}{dt} = -I_{ion}(V_i, \ldots) - g_{syn}(V_i - V_{syn}) + \epsilon g_{syn} S_j (V_i - V_{syn}). \qquad (2.17)$$

Note that if we set $\epsilon = 0$, the two neurons are decoupled. In other words, slowly decaying synapses behave like weak synapses. We have assumed that $g_{syn} > G^*$, so that the neurons are oscillating; thus, we have a system of two weakly coupled oscillators. The theory of averaging implies that the behavior of the coupled cells is determined by a pair of phase equations. That is, $V_i(t) = V(\theta_i) + O(\epsilon)$ where V satisfies

$$C\frac{dV}{dt} = -I_{ion}(V, \ldots) - g_{syn}(V - V_{syn})$$

and is the unique $T-$periodic solution found for $g_{syn} > G^*$.

A Brief Digression. Before continuing, we briefly review the theory of weakly coupled oscillators. Consider a pair of identical mutually coupled oscillators,

$$X_1' = F(X_1) + \epsilon C(X_1, X_2) \quad X_2' = F(X_2) + \epsilon C(X_1, X_2),$$

where $\epsilon \ll 1$. We define:

1. $X_0(t)$ is the unique phase asymptotically stable P-periodic function to $X' = F(X)$;
2. $X^*(t)$ is the unique solution to

$$U'(t) = -(D_X F(X_0(t)))^T U(t) \qquad U(t) \cdot X_0'(t) = 1,$$

where A^T is the transpose of A. $X^*(t)$ is called the adjoint solution to the linearization around the limit cycle.

Then for ϵ small, we can apply averaging to the coupled system, and we find that $X_{1,2}(t) = X_0(\theta_{1,2}) + O(\epsilon)$ where

$$\theta_1' = 1 + \epsilon H(\theta_2 - \theta_1)$$
$$\theta_2' = 1 + \epsilon H(\theta_1 - \theta_2)$$

and

$$H(\phi) = \frac{1}{P} \int_0^P X^*(t) \cdot C(X_0(t + \phi), X_0(t))\, dt.$$

We can apply these averaging results to the present problem. We note that the coupling is only through the potentials, $V_i(t)$, so that the term that defines H is a scalar product. The phases, θ_i, of the two oscillators evolve according to the equations

$$\theta_1' = 1 + \epsilon H(\theta_2 - \theta_1) \quad \theta_2' = 1 + \epsilon H(\theta_1 - \theta_2), \tag{2.18}$$

where

$$H(\phi) = -\frac{g_{syn}}{T} \int_0^T V^*(t) \hat{S}(t + \phi)(V_{syn} - V(t))\, dt, \tag{2.19}$$

where $V^*(t)$ is the voltage component of the adjoint. The function $Z(t) \equiv V^*(t)(V_{syn} - V(t))$ is closely related to the phase-response curve (PRC) for the oscillator. It vanishes when the neuron fires and is nonnegative between spikes. Figure 6C shows both the adjoint, $V^*(t)$, and $Z(t)$ for a model neuron. The function $\hat{S}$ satisfies

$$\frac{d\hat{S}}{dt} = 1 - K(V(t))\hat{S}. \tag{2.20}$$

Figure 6B shows $\hat{S}$ for the model. Let $\phi = \theta_2 - \theta_1$ denote the phase difference between the two neurons. Then

$$\frac{d\phi}{dt} = \epsilon(H(-\phi) - H(\phi)) \equiv G(\phi).$$

Clearly, $G(0) = 0$ so that the synchronous solution is a fixed point, and there is a synchronous solution to the coupled system. It is stable if $G'(0) < 0$. From the definition of G, we see that synchrony is stable if and only if $-2H'(0) < 0$ or $H'(0) > 0$. From equation 2.19,

$$H'(0) = -\frac{g_{syn}}{T}\int_0^T Z(t)\hat{S}'(t)\,dt. \tag{2.21}$$

We now show that we can expect $H'(0) < 0$. To do this, we want to show that the integral is positive. We first consider $Z(t)$. For type 1 neurons, the voltage adjoint, $V^*(t)$ is positive (Hansel et al., 1995; Ermentrout, 1996; Izhikevich, 1999) and vanishes at $0, T$. Since the synapses are excitatory, $V(t) < V_{syn}$ except perhaps when the neuron spikes. Thus, $Z(t) = V^*(t)(V_{syn} - V(t))$ is positive except, perhaps, for a small amount of time near $t = 0$ and $t = P$. Now consider $\hat{S}'(t)$. The function $K(V(t))$ vanishes when the neuron is away from the peak of its action potential. From equation 2.20, we see that in a neighborhood of the spike, $\hat{S}'(t)$ is sharply negative, but during the rest of the period, $\hat{S}'(t) = 1$. During the spike, $Z(t)$ is nearly zero and perhaps even negative. Thus, the product $Z(t)\hat{S}'(t)$ is positive over the majority of the period of the oscillation so the integral is positive and $H'(0) < 0$. This means that synchrony is unstable. Figure 6D shows the numerically computed function $H(\phi)$ for the biophysical model; clearly $H'(0) < 0$, as dictated by this simple argument.

Since $G(\phi)$ is a continuous odd periodic function, it also has a fixed point at $T/2$ corresponding to the antiphase solution. The antiphase state is stable if and only if

$$H'\left(\frac{T}{2}\right) = -\frac{g}{T}\int_0^T Z(t)\hat{S}'\left(t + \frac{T}{2}\right)\,dt$$

is positive. Now, in contrast to the synchronous case, the steep negative slope of $\hat{S}(t)$ occurs during the part of $Z(t)$ where it is nearly maximal. Thus, the integral could be negative, implying stability of the antiphase state. This is not so clear-cut as the instability of synchrony; however, Figure 6D shows very clearly that the slope of $H(\phi)$ is positive at $T/2$ so that synchrony is stable.

2.2.1 Comparison with Slow Coupling. Frankel and Kiemel (1993) and more recently Izhikevich and Hoppensteadt (in press) studied a similar

class of models but instead replace equation 2.16 with

$$\frac{ds}{dt} = \epsilon[K(V)(1-s) - s].$$

(In fact, both use a more general form of coupling, but for purposes of discussion, we will consider this simple example.) They assume that there is a pair, $(V_0(t), s_0)$, such that when $s = s_0$ in the membrane equation, there is a periodic solution $V_0(t)$ with period, T, such that

$$s_0 = (1-s_0)\int_0^T K(V_0(t))\, ds.$$

They then expand around this fixed point of the averaged equation, $s_j = s_0 + \epsilon u_j$, and obtain two equations for each oscillator: one for the phase of the oscillation (as above) and one for the perturbation, u_j. If the oscillators are identical and mutually coupled only through the voltages as above, then equations have the form

$$\begin{aligned}
\theta_1' &= h(\theta_2 - \theta_1) + cu_2 \\
\theta_2' &= h(\theta_1 - \theta_2) + cu_1 \\
u_1' &= -bu_1 + k(\theta_2 - \theta_1) - \gamma - h'(0)u_2 \\
u_2' &= -bu_2 + k(\theta_1 - \theta_2) - \gamma - h'(0)u_1
\end{aligned}$$

where the coefficients are:

$$\begin{aligned}
c &= \frac{g}{T}\int_0^T Z(t)\, dt \\
h(\phi) &= \frac{g}{T}\int_0^T Z(t)\Lambda(t+\phi)\, dt \\
k(\phi) &= \frac{g}{T}\int_0^T \Lambda'(t)Z(t)\Lambda(t+\phi)\, dt \\
\gamma &= \frac{1}{T}\int_0^T [\alpha(V(t)) + 1]\Lambda(t)\, dt \\
b &= \frac{1}{T}\int_0^T [\alpha(V(t)) + 1]\, dt \\
Z(t) &\equiv V^*(t)(V_{syn} - V(t)) \\
\Lambda(t) &\equiv \int_0^t [\alpha(V(t'))(1-s_0) - s_0]\, dt'
\end{aligned}$$

(These calculations are derived in Izhikevich & Hoppensteadt, in press, for the general case.) We note the quantity, $Z(t)$, which again appears as in our previous calculations. We recall that $Z(t)$ is positive except, perhaps, for a small region near the spike. The function $\Lambda(t)$ vanishes at 0 and T, and for t slightly larger than zero (after the spike), $\alpha(V(t))$ is essentially zero; thus, $\Lambda'(t)$ is negative for most of the period. Since $\Lambda(T) = 0$, this function must have the following shape. It starts at zero, the time of the spike, rises quickly, and then linearly decreases to zero. Its derivative is positive for a short period of time during the spike, and then for the remainder of the period, $\Lambda'(t) = -s_0$ is negative. Thus, we can conclude the following about the functions:

- $c > 0$ since $Z(t)$ is positive except near the short-lasting spike.
- $h'(0) \equiv f < 0$ since

$$h'(0) = \frac{g}{T} \int_0^T Z(t)\Lambda'(t)\, dt,$$

  and this is negative since $\Lambda'(t)Z(t)$ is negative after the spike.

- $k'(0) \equiv d > 0$ since

$$k'(0) = \frac{g}{T} \int_0^T [\Lambda'(t)]^2 Z(t)\, dt,$$

  and the integrand is positive over most of the interval.

- $b > 0$ since the integrand is everywhere positive.

With these heuristic observations, we can determine the stability of the synchronous state. Subtracting the phase equations, $\phi = \theta_2 - \theta_1$, the third-order system is obtained:

$$\begin{aligned}
\phi' &= c(u_1 - u_2) + h(-\phi) - h(\phi) \\
u_1' &= k(\phi) - \gamma - h'(0)u_2 - bu_1 \\
u_2' &= k(-\phi) - \gamma - h'(0)u_1 - bu_2.
\end{aligned}$$

The synchronous state satisfies $\phi = 0$,

$$u_1 = u_2 = \frac{k(0) - \gamma}{b + h'(0)}.$$

In the regrettable case that the denominator is zero (which is possible since $b > 0$ and $h'(0) < 0$), there is no synchronous state. Assuming that the denominator is nonzero, we can check the stability of the synchronous state.

The linearization is

$$M = \begin{bmatrix} -2f & c & -c \\ d & -b & f \\ -d & f & -b \end{bmatrix}.$$

The characteristic polynomial can be easily factored:

$$\chi(\lambda) = (\lambda + b - f)(2f(f+b) - 2dc + (b+3f)\lambda + \lambda^2).$$

Since $f < 0$ and $b > 0$, there is at least one negative real root. Consider the second factor. The roots of this have negative real parts if and only if the coefficients are positive. Thus, if $b + 3f < 0$, then synchrony is unstable. Suppose to the contrary that $b + 3f > 0$. Since $f < 0$, then $b > -f$, so that $f(b+f) < 0$, and thus the constant coefficient is negative since $dc > 0$. Thus, we conclude that synchrony is also unstable with synapses that both slowly rise and slowly decay.

The existence of the antiphase state is clear. We know that there is a root, $T/2$ to $h(-\phi) - h(\phi) = 0$, corresponding to the antiphase solution. From the ϕ' equation, this implies that $u_1 = u_2$. The $u_{1,2}$ equations imply that this can be a fixed point only if $k(-T/2) = k(T/2)$. However, this is true since $k(t + T) = k(t)$. Stability of the antiphase solution can likewise be determined. The linearization factors to

$$\chi(\lambda) = (\lambda + b - f)(2g(f+b) - 2ec + (2g + f + b)\lambda + \lambda^2),$$

where

$$g = h'(T/2) = \frac{1}{T}\int_0^T Z(t)\Lambda'\left(t + \frac{T}{2}\right)\, dt$$

$$e = k'(T/2) = \frac{1}{T}\int_0^T \Lambda'(t)Z(t)\Lambda'\left(t + \frac{T}{2}\right)\, dt.$$

As above, since $f < 0$ and $b > 0$, there is at least one negative root. For stability of the antiphase solution, we require $2g + f + b > 0$, so that if g is large enough and positive (as it was for the fast-rising, slow-decaying case), then this will hold. However, $f + b$ could be negative, so for stability, we need ec to be negative enough. Since $c > 0$, this means $e = k'(T/2)$ should be negative. Thus, as in the slow-decay case, the stability of antiphase solutions seems possible but is not qualitatively guaranteed.

3 Networks with Slowly Decaying Synapses

One of the main reasons that slow synapses have been of recent theoretical interest is that their persistence enables one to maintain spatially localized

structures that have been used as models for working memory. In this section, we first consider a single layer of cells with recurrent connections and slowly decaying synapses. We consider a purely excitatory network and show the existence of traveling fronts of activity. We show that it is possible to estimate the speed of propagation of wave fronts by solving a particular boundary value problem. Next, we show that if the connections have local excitation and long-range inhibition (the standard assumptions for pattern formation), then the velocity of the fronts above tends to zero as the inhibition increases and further increases of the inhibition lead to localized structures for any type I biophysical model. The interesting point about this is that with fast-rising and slow-decaying synapses, the resulting model looks just like the classic Amari model.

The general spatially discrete network has the following structure:

$$C\frac{dV_j}{dt} = -I_{ion}(V_j, \ldots) - \sum_k J^e(j-k)s_k(t)(V_j - V^e) - \sum_k J^i(j-k)s_k(t)(V_j - V^i), \tag{3.1}$$

where $J^{e,i}(l)$ is the synaptic conductance magnitude of a connection between two cells that are l units apart, $V^{e,i}$ are the reversal potentials of the excitatory and inhibitory synapses, and $s_k(t)$ are the synapses satisfying

$$\frac{ds_j}{dt} = \alpha(V_j)(1 - s_j) - \epsilon s_j. \tag{3.2}$$

We have (somewhat unrealistically) lumped the inhibitory and excitatory interactions together. That is, rather than having a distinct population of inhibitory neurons, we have assumed that the inhibition is instantaneous and gated by the excitatory neurons. Such reductions to single-layer models have a long history going back to Amari (1977) but usually in the context of firing-rate models (however, see Gutkin et al., 2001 or Wang, 2001, for examples of spiking models with lateral inhibitory coupling). For the purposes of analysis, we will consider the continuum analog of this discrete coupling where the sums are replaced by integrals:

$$\int_\Omega J^{e,i}(x-y)s(y,t)\,dy.$$

In numerical experiments, we obviously consider the discrete network and choose the sums to extend only as far as the network exists. For analysis, we will consider an infinite domain. (Note that this is clearly a requirement to study wave propagation but unneccesary for localized structures.)

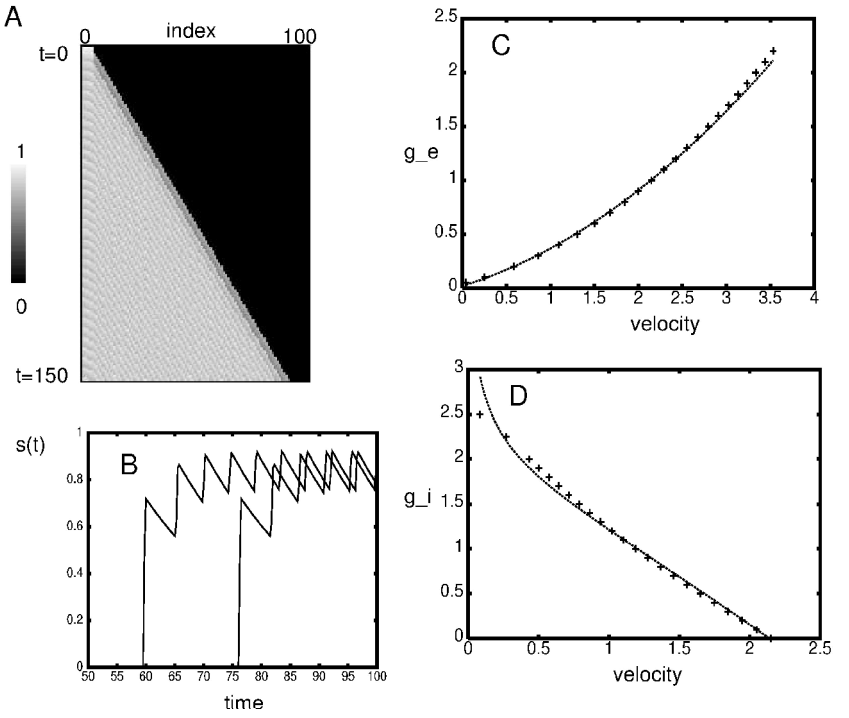

Figure 7: Wave front provided by synaptically coupling a network of 100 conductance-based model neurons with excitatory synapses. All cells are started at rest. The synaptic variables, s_j, of the first five cells are set to 1 to initiate the wave. (A) The space-time behavior of the synaptic gating variables, s_j. (B) The behavior of $s_{40}(t)$, $s_{50}(t)$. (C) The velocity as a function of the strength of the coupling, g_e. Velocity is measured by computing the times when s_{40}, s_{50} are 0.5. The velocity is 10 divided by the time difference. The solid curve is a theoretical approximation. (D) The velocity versus inhibitory coupling for the network with lateral inhibition along with a theoretical approximation (see the next section.)

3.1 Wave Fronts. In this section, we assume there is no inhibition. There have been a number of experimental studies of wave propagation in cortical slices in which the inhibition is pharmacologically blocked (Golomb & Amitai, 1997; Pinto & Ermentrout, 2001b). Later, we extend the analysis to the case where the inhibition is nonzero. We begin with a simulation of a wavefront to illustrate the phenomena. Figure 7A shows the evolution of the synaptic gating variable, s_j, for a biophysical model with 100 cells. The time constant of the synapse is 20 msec (corresponding to $\epsilon = .05$). The wave is initiated by turning on the synapses of the first five cells. The velocity of the front is 1/1.72 cells per millisecond, and the asymptotic period of the

oscillations in the wake of the front is 4.50 milliseconds. The average of the synaptic gating variable, $\bar{s}$, is 0.836. Arguments such as given in the previous sections allow us to self-consistently determine the steady-state frequency and mean value of the synapse. However, since we have no explicit equation for the frequency-current curve, we simply substitute $\bar{s}$ into the membrane equation and explicitly compute the period; that is, we numerically solve

$$CdV/dt = -I_{ion}(V, w) - g\bar{s}(V - V_{syn})$$

and find the period from this. The value we obtain is 4.45 milliseconds, which is quite good. Repeating the same calculation for $\epsilon = .01$, a 100 msec time constant for the synapse, we numerically find $\bar{s} = 0.965$, and the period of the oscillations in the wake of the front is 4.10 msec. The period from the single cell using the above value of $\bar{s}$ is 4.10 msec.

Figure 7B shows the behavior of the synaptic gating functions for two different cells. Both have the same characteristic rise followed by low-amplitude fluctuations around a mean value. Figure 7C shows the velocity of the fronts as a function of the strength of the excitatory coupling. There are several approaches that we could take to estimate analytically the velocity of network using the approximation of slowly decaying synapses.

One approximation that comes to mind is the same as used in Chen, Ermentrout, and Wang (1998) and is valid if the synapses are both slowly rising and slowly decaying. That is, we analyze

$$\frac{\partial s}{\partial t} = aF\left[g\int_{-\infty}^{\infty} J(x-y)s(y,t)\,dy\right](1-s) - s/\tau_{syn},$$

where F is the firing rate as a function of the total synaptic conductance (which we earlier approximated with a square root; cf. equation 2.14). This is of questionable validity when the synapses are rapidly rising. Furthermore, we are left with solving a nonlinear integral equation. Replacing the firing rate F with a step function makes it possible to compute the velocity of fronts explicitly (Chen et al., 1998) however this turns out to be a very bad approximation for our problem. (There are two possible reasons: a step function is not particularly close to the square root or the approximation of slow-rising synapses is not very good.)

An alternative approach is suggested by Figure 7B, we note that $s(t)$ is well aproximated by

$$S(t) \approx s_{\max}(1 - \exp(-bt)), \tag{3.3}$$

where b, $s_{\max}$ are chosen to fit the profiles shown in the figure and t is the time after the neuron associated with the variable s crosses some prescribed voltage, V_T. (For example, we might take V_T as the voltage at which point $\alpha(V)$ in equation 3.2 is half its maximum.) Here we have exploited two aspects of

the model: slow decay, so there is little modulation, and saturation, so that the synapses do not increase without bound. With this approximation, we need to solve the following equation:

$$C\frac{\partial V}{\partial t} = -I_{ion} - g_e\left(\int_{-\infty}^{\infty} J(x-y)S(t-t^*(y))\,dy\right)[V(x,t)-V^e],$$

where $t^*(x)$ is the time at which the neuron at x first fires. When we say "solve" this, we mean that we seek a traveling wave solution, $t^*(x) = x/\nu$, where ν is the velocity and $V(x,t) = U(\nu t - x)$. We require $U(-\infty) = V_{rest}$ and $U(0) = V_T$, where V_T is as above. Additionally, we have equations for all the gating variables, and they must be at rest at $-\infty$. This approach was taken in Ermentrout (1998b) in order to find traveling waves for synaptically coupled membrane models that elicited exactly one action potential. In contrast, here we assume that the neuron fires infinitely many times once it crosses threshold. Since this model does not admit a simple closed-form solution, we still must solve a nonlinear boundary value problem. This can be done using AUTO (Doedel, 1981) by either treating the problem on a large finite domain or using the boundary-projection method. In Ermentrout (1998b), we observed that the simple integrate-and-fire model provides a fairly good approximation for the single-spike system We thus try that here as well. The integrate-and-fire model has the form:

$$\frac{1}{a}\frac{\partial V(x,t)}{\partial t} = -V(x,t) - R_m I_{syn}(x,t), \tag{3.4}$$

where

$$I_{syn} = g_e(\bar{V} - V^e)\int_{-\infty}^{\infty} J_e(x-y)S(t-t^*(y))\,dy. \tag{3.5}$$

$1/a$ is the membrane time constant of the neuron, R_m is the bulk resistance, and $V^e - \bar{V}$ is the difference between some average potential and the synaptic drive. ($\bar{V}$ could be chosen as the resting potential, but that is not accurate especially when the cell is firing, so we allow it to be a "free" parameter.) For the integrate-and-fire model, we define $t^*(x)$ to be the time at which the potential of the cell at $x = x^*$ reaches a prescribed value, V_T. Integrating equation 3.4, we obtain the following system,

$$V_T = R_m g_e s_{\max}(V^e - \bar{V})\int_{-\infty}^{\infty} J_e(x-y)G(t-t^*(y))\,dy,$$

where

$$G(t) = \frac{1}{b-a}(a(1-e^{-bt}) - b(1-e^{-at})). \tag{3.6}$$

We look for solutions to this of the form $V(x,t) = U(\nu t - x)$ with $U(-\infty) = 0$ and $U(0) = V_T$. For $J(x) = \exp(-|x|/\sigma)/(2\sigma)$ (as well as many others), this is easy to solve. Plugging this form into the equation just before equation 3.6, we obtain

$$g^* \equiv \frac{V_T}{R_m(V^e - \bar{V})s_{max}} = g_e \int_0^\infty J(y)G(y/\nu)$$

$$= g_e \frac{\sigma^2 ab}{(\nu + b\sigma)(\nu + a\sigma)} \equiv g_e F(\nu, a, b, \sigma). \qquad (3.7)$$

Without loss of generality, we set $\sigma = 1$ since we can easily rescale the spatial interactions. It is simple to solve this equation for the velocity, ν, but before doing this, we make a few remarks. First, F is monotonically decreasing as a function of ν, so that for each value of $g_e > g^*$, there is a unique velocity for the front. This contrasts with the single-spike case, where there are two values of the velocity, ν, for each $g_e > g^*$. The monotonicity of F can be traced to the monotonicity of the synaptic gating variable, $S(t)$, in the present case, which implies that $G(t)$ is monotone. (In fact, $G'(t) > 0$.) Clearly, if $J(y) \geq 0$, $\partial F/\partial \nu < 0$ for all positive ν, so F is monotone. For the single spike wave (and for wave packets which spike finitely many times), the synaptic conductance envelope, $S(t)$ is nonmonotone, so we can expect F to be nonmonotone in general. Second, as g approaches g^* from above, the velocity of the front tends to zero ($F(0,\cdot) = 1$). Again, this contrasts with the finite spike case where the wave terminates at a finite nonzero velocity. Finally, we remark that at very low velocities, we expect that the approximation for $S(t)$ will break down since the time between successive voltage spikes will increase, allowing the synaptic gates, $s(t)$ to relax to zero. This will be a problem only if the velocity, ν, and the decay of the synapses, ϵ, are roughly the same order of magnitude. The detailed asymptotics in this case remain to be done; we expect them to be very difficult since we can no longer approximate $s(t)$ by the envelope, $S(t)$. In Osan, Curtu, Rubin, and Ermentrout (in press), two-spike, three-spike, and infinite-spike wavefronts have been calculated for the integrate-and-fire models. For the multiple-spike solutions, a series of complicated algebraic expressions is derived. For the infinite-spike case, the velocity of the front is required in order to solve the equations for the spike times. A related calculation was done for integrate-and-fire models, where $J_e(x)$ has finite support (Osan, Rubin, Curtu, & Ermentrout, in press).

Returning to the velocity relationship, equation 3.7, for the integrate-and-fire model and assuming that $\sigma = 1$, we can easily solve for g_e to obtain a relationship between g_e and ν:

$$g_e = \frac{g^*}{F(\nu, a, b, 1)}.$$

There are two free parameters, a and g^*; the parameter b is specified from the synaptic rise time. The two free parameters have a nice intuitive meaning: $1/a$ is the effective membrane time constant, and g^* is the minimal conductance required to induce repetitive firing of the neuron. Figure 7C shows the numerically computed velocity as a function of the synaptic strength for the full conductance-based model and the approximation from the integrate-and-fire model using $g^* = 0.0194, a = 2.5, b = 0.08$. The agreement is excellent over the whole range of values of g. (The fit was done manually with an effort to make the theoretical value at $g_e = 1$ match closely.) We close with the following remarks.

If we change the synaptic time constant from 20 to 100, we find that the velocity does not change very much at all. This is to be expected since the rise time does not change; only the parameter $s_{\max}$ should be altered by the change in the time constant. At a fixed firing frequency, F,

$$s_{\max} = \frac{aF}{aF + 1/\tau_{syn}},$$

so that we would expect changes in $s_{\max}$ only when F is very small.

If, however, we decrease the decay rate to 2 milliseconds (the approximate decay rate of fast AMPA synapses), then the theory provides a very bad estimate of the velocity. The theory depends strongly on the fact that the synapses remain close to saturation once they have become activated. If synapses decay quickly, then the approximation in equation 3.3 does not hold. This changes the form of equation 3.7, so that it becomes similar to the "single-spike" assumption for travelling waves made in Ermentrout (1998b) and Golomb and Ermentrout (2001). One of the main theoretical differences between propagating fronts and propagating pulses is that the existence of fronts disappears at zero velocity (cf. Figures 7C and 7D). The existence of propagating pulses disappears at a finite nonzero velocity, which depends on the details of the spatial interaction function among other things.

3.2 Inhibition and the Transition to Localized Structures. In the analysis of the waves, we assumed that $W^i(x) = 0$, so that there was no inhibition. The analysis of the conductance-based model as well as the integrate-and-fire approximation can just as easily be done with the inhibition included. Consider the synaptic current:

$$I_{syn} = g_e \left[\int_{-\infty}^{\infty} J_e(x-y)s(y,t)\,dy \right] (V(x,t) - V^e) + g_i \left[\int_{-\infty}^{\infty} J_i(x-y)s(y,t)\,dy \right] (V(x,t) - V^i). \tag{3.8}$$

We can again solve the network equations to compute the velocity as a function of the parameter g_i for fixed values of all the other parameters.

Alternatively, we can solve a boundary value problem for the wave using the synaptic gate, $s(t) = S(t) \equiv s_{\max}(1 - \exp(-bt))$. Figure 7D shows the wave velocity computed in a network of 160 cells as the inhibition g_i varies. To gain some insight into the shape of this curve, we again appeal to the simple integrate-and-fire model, equation 3.4 with

$$I_{syn} = g_e(\bar{V} - V^e) \int_{-\infty}^{\infty} J_e(x-y) S(t - t^*(y))\, dy + g_i(\bar{V} - V^i) \int_{-\infty}^{\infty} J_i(x-y) S(t - t^*(y))\, dy.$$

As before, we solve this for the traveling wave front and obtain a relationship between the velocity, v, and the various parameters:

$$g^* \equiv \frac{V_T}{R_m(V^e - \bar{V}) s_{\max}} = g_e F(v, a, b, 1) - g_i r F(v, a, b, \sigma),$$

where F is defined in equation 3.7 and $r = (V^e - \bar{V})/(\bar{V} - V^i)$. Here, σ is the space constant for the inhibitory interaction (with the excitatory set to 1). We can solve this for g_i to obtain a relationship between the velocity and the inhibitory conductance:

$$g_i = \frac{g_e F(v, a, b, 1) - g^*}{r F(v, a, b, \sigma)}.$$

Using the values for g^*, a, b from Figure 7C, we have one adjustable parameter, r, the ratio of the effective driving potentials of the inhibitory to excitatory synapses. Adjusting r manually, we find that $r = 0.24$ fits all but the lowest-velocity values quite well, as can be seen from Figure 7D. For $V^e = 0$, $V^i = -80$, this value of r corresponds to $\bar{V} = -64.5$, which is just slightly more depolarized than the rest state of the biophysical model. The critical amount of inhibition that stops the wave (that is, $v = 0$) is

$$g_i^{v=0} = (g_e - g^*)/r.$$

This is independent of the space constant of the inhibition as well as the temporal parameters, a, b. Naturally, for synapses that do not have slow decay, this approximation breaks down.

Remark. The inhibition that we have considered here is "instantaneous" (there is no subpopulation of inhibitory cells) and has a longer range than the excitation. The lack of dynamics for the inhibition as well as the fact that we consider only fronts and not traveling pulses are likely reasons for the

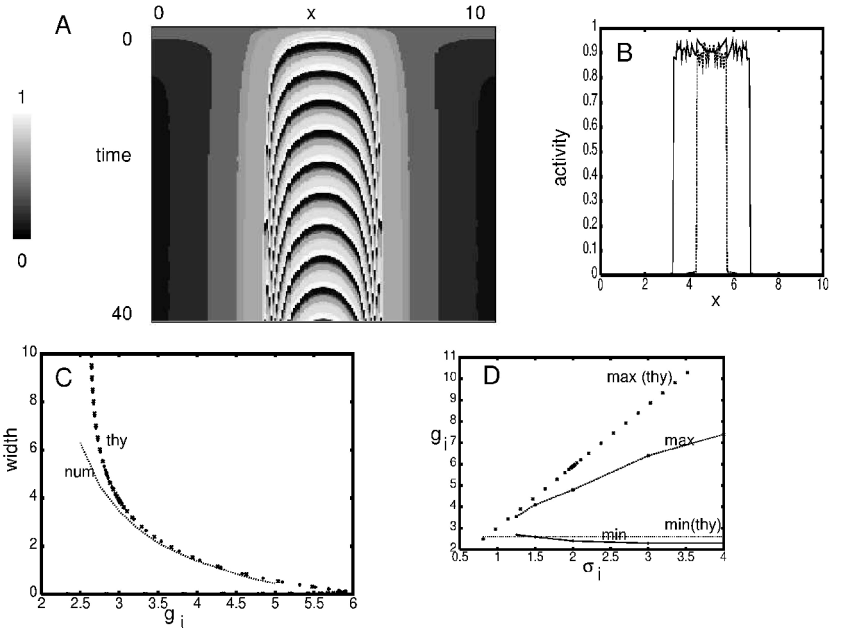

Figure 8: Localized structures in the biophysical model. (A) The space-time evolution of the synaptic gating variables, $s(x, t)$, for a network of 200 cells in a domain of length 10 ($\delta x = 0.05$). All cells are started at rest except the synaptic variables, $s(x) = \exp(-(x-5)^2)$. Parameters are $g_e = 1, g_i = 3, \sigma_e = 1, \sigma_i = 2$. (B) A time slice of $s(x, t)$ at $t = 36$ for two different inhibitory conductance strengths, $g_i = 3, 4$. The larger the inhibition, the narrower the width. (C) How the width varies as a function of g_i, with $g_e = 1, \sigma_e = 1, \sigma_i = 2$. The dotted line is the theoretical curve found by solving two algebraic equations. (D) The minimum and maximum allowable amounts of synaptic inhibition vary with the inhibitory space constant.

lack of multiple stable wave speeds observed in Golomb and Ermentrout (2001).

What happens for $g_i > g_i^{\nu=0}$? It turns out that for slowly decaying synapses, the loss of traveling waves coincides with the emergence of localized regions of activity. We now turn to an analysis of these localized structures (bumps) in the model with lateral inhibition. In many ways, these are simpler to analyze than the waves since the structures are stationary. Figure 8A shows the evolution in space and time of a localized structure for equation 3.1. Here, the domain in the interval [0,10] divided into 201 cells of width 0.05. The interaction kernels are normalized exponentials, $W^z(x) = \exp(-|x|/\sigma_z)/(2\sigma_z)$, for $z = e, i$. We choose $\sigma_e = 1$ without loss in generality. For initial data of various widths, the system evolves into a local

structure with a constant width independent of the initial data. However, the width is strongly dependent on the strength of the inhibition and the width of the inhibitory interactions. Figure 8B shows a plot of the spatial profile of $s(x, t)$ for two different values of the inhibitory conductance, g_i. Figure 8C shows the width of the structure as a function of the inhibition over a range of conductances. There is a minimal value of g_i, say, $g_i^{\min}$, below which we find that the structure occupies the whole domain. There is also a maximal value, say, $g_i^{\max}$, above which the network collapses to the stable equilibrium point. Figure 8D shows how the minimum and maximum conductances depend on the inhibitory space constant. The minimum value, $g_i^{\min}$, is nearly independent of the space constant, while the maximum varies nearly linearly.

As with wave fronts, if the synapses decay slowly but rise quickly, then when a neuron, j, is firing, $s_j \approx 1$, and when the neuron is not firing, $s_j = 0$. Thus, the synaptic gates are almost piecewise constant, at least in the limit as $\epsilon \to 0$. This makes the analysis of this equation considerably easier than in the case for which the rise time and the decay time are slow (Ermentrout, 1994; Bressloff & Coombes, 2000). Then it is necessary to perform averaging, and one gets a complex nonlinear equation for the synapses.

We discuss the analysis of the present model by taking the continuum limit. We first briefly review the analysis of Amari (1977) so that it is easy to see the similarity of our methods. Amari was interested in stationary solutions to

$$u_t(x, t) + u(x, t) = \int_{-\infty}^{\infty} W(x - y)H(u(y, t) - \theta)\, dy,$$

where $W(x)$ is of the form shown in Figure 9A and $H(u)$ is the Heaviside step function. He supposes that $u(x) > \theta$ for $x \in [0, M]$ and $u(x) < \theta$ on the rest of the line. Continuity implies that $u(0) = u(M) = \theta$, which leads to the equation

$$\theta = \int_0^M W(y)\, dy \equiv Q(M).$$

(Note that $u(0) = u(M)$, so there is actually only one equation to solve.) As seen in Figure 9B, for a range of threshold values, θ, there are two possible roots to this. Amari showed that only the larger root is stable. We emphasize that in order for the function Q to be nonmonotone, it is necessary that the inhibition extend further than the excitation. Without this assumption, there will be only one possible width (since Q is monotone), and this root is unstable.

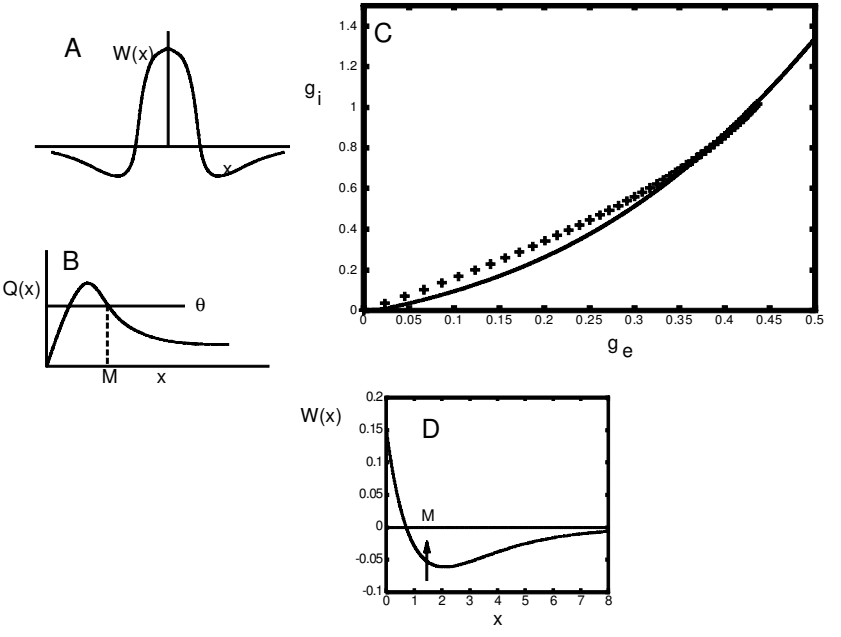

Figure 9: The Amari construction of localized structures in the continuous piecewise-constant model, $u(x) = \int_{-\infty}^{\infty} W(x-y)H(u(y)-\theta)\,dy$, and its analog in the biophysical system. (A) The interaction kernel, $W(x)$, for the Amari model. (B) The solution to $Q(x) \equiv \int_0^x W(y)\,dy = \theta$ for the bump width, M. (C) The two-parameter bifurcation curve for the biophysical model (solid line) and the cumulative sums for finding the width (see the text). (D) The interaction kernel and the relative position of the width.

With these preliminaries, we are interested in solutions to

$$C\frac{\partial V(x,t)}{\partial t} = -I_{ionic}(V,w) - I_{syn}(x,t),$$

where $I_{syn}(x,t)$ is as in equation 3.8. We seek solutions to this in which neurons in the interval $[0,M]$ are active and neurons outside this interval are at rest. For a neuron at rest, $s(x,t) = 0$. Thus, the synaptic current felt by a neuron at x is

$$I_{syn}(x,t) = g_e\left[\int_0^M J_e(x-y)s(y,t)\,dy\right](V(x,t)-V^e) + g_i\left[\int_0^M J_i(x-y)s(y,t)\,dy\right](V(x,t)-V^i), \tag{3.9}$$

where J_e, J_i are the normalized interaction functions defined previously. We now exploit the fact that the synapses decay slowly. This implies (as above), that $s(x, t) \approx s_{\max}$ for all $x \in [0, M]$, so that equation 3.9 is

$$I_{syn}(x, t) = s_{\max}[g_e Q_e(x, M)(V(x, t) - V^e) + g_i Q_i(x, M)(V(x, t) - V^i)],$$

where

$$Q_{e,i}(x, M) = \int_0^M J_{e,i}(x - y)\, dy.$$

In order to find M, we need an additional condition. We ask how a neuron goes from rest to repetitive activity. In the models that we have analyzed here, this occurs through a saddle-node bifurcation in which the rest state is lost. Thus, we want neurons within the localized activity to have no stable fixed point and neurons outside the "bump" to be at rest. This implies that we must choose M so that $I_{syn}(M, t)$ lies on the curve of saddle-node points for the biophysical model. There are at least two ways to solve this. Consider the following equation,

$$C\frac{dV}{dt} = -I_{ion}(V, w) - G_e(V - V^e) - G_i(V - V^i),$$

where $G_{e,i}$ are constants. We assume that when $G_e = G_i = 0$, this system has a stable rest state. As G_e increases, the rest state is lost at a saddle node. For each G_i, there is a G_e for which the fixed point is on a saddle-node point. Figure 9C shows the curve of saddle nodes as computed using AUTO for our biophysical equation. Now consider the curve parameterized by M,

$$\Gamma(M) = (s_{\max} g_e Q_e(M, M), s_{\max} g_i Q_i(M, M)).$$

We want $\Gamma(M)$ to intersect the saddle-node curve. Figure 9C shows $\Gamma(M)$ at discrete values of M, indicating a crossing at about $M = 1.45$. Thus, we see that formally, the construction of bumps in ionic models with slowly decaying synapses is identical to Amari's construction; the curve of saddle-node points defines the threshold for firing, and the curve $\Gamma(M)$ plays the role of $Q(M)$ in Figure 9B. The width of the bump as a function of some parameter such as g_i can be computed in the following manner. From the numerical calculation of the curve of saddle-node points, we obtain a parameterization, $(G_e(\lambda), G_i(\lambda))$, which we can interpolate to form a smooth curve. The width of the bump is found by solving the two equations in two unknowns, (M, λ):

$$\begin{aligned} s_{\max} g_e Q_e(M, M) &= G_e(\lambda), \\ s_{\max} g_i Q_i(M, M) &= G_i(\lambda). \end{aligned} \tag{3.10}$$

We have done this using the curve computed in Figure 8B, with the results of the width as a function of g_i shown in Figure 8C. The agreement with the numerically computed widths (found by integrating a network of 400 cells and measuring the width) is very good, particularly given that the time constant of the synapse is only 20 milliseconds, so that the synaptic gates have fairly large temporal fluctuations near the edges of the bump. We point out two important features of the analytic calculation.

First, as g_i decreases to a fixed value, the width of the bump goes to infinity. As M tends to infinity, $Q_e(M, M) = Q_i(M, M) = 1/2$ independent of σ_i, the space constant of the inhibition. Thus, the minimum value of the inhibitory conductance supporting bumps is independent of the space constant. Figure 8D shows the constant value of g_i where this occurs; it is quite close to the value determined by simulating the full network. Importantly, we note that the minimum allowable value of g_i for the existence of a bump appears to coincide with the maximum value of g_i which allows for traveling wave fronts.

Second, as g_i increases, the bump disappears at a saddle-node point. This is analogous to crossing the peak of $Q(x)$ in Figure 9B. Unlike the minimal value of g_i, the maximum value of g_i is expected to depend on σ_i. Using the interpolated curve for $(G_e(\lambda), G_i(\lambda))$, we can follow the two-parameter curve using g_i and σ_i as parameters to get the maximum value of g_i as a function of σ_i. This leads to the curve shown in Figure 8D. The curve agrees at least qualitatively with the numerically computed curve. Since this is the curve of points for which the width of the bump is minimal, it means that the cells inside the bump are getting relatively small excitation. Thus, they are firing at low rates compared to cells that are in a bump far from criticality. Thus, we expect that the effective synaptic excitation maintaining the bump is far less than $s_{\max}$ so that the theory is expected to predict a much greater amount of inhibition required to kill the bump.

An alternate way to compute the bump width is to solve directly the steady-state equations for the full biophysical model with

$$I_{syn} = g_e s_{\max} Q_e(M, M)(V(x, t) - V^e) + g_i s_{\max} Q_i(M, M)(V(x, t) - V^i).$$

To see how the width varies with g_i, we start with g_i large and M fixed at some value. We find the fixed points for the full ionic model. We then follow this as a function of g_i with M fixed until a saddle node is found. Then we follow the curve of saddle nodes in the two-parameter plane (g_i, M). This is shown in Figure 8C. The agreement with our first method is almost exact. This method has the disadvantage of making it very difficult to compute the maximum amount of inhibition as a function of σ_i since we have to compute a three-parameter curve using g_i, M, and σ_i.

We can construct bumps in the integrate-and-fire model as we computed the waves. Here, the computations are much simpler since we need only

look at steady-state potentials. That is, we determine the width of the bumps by requiring that

$$V_T/R_m = g_e s_{\max} Q_e(M, M)(V^e - \bar{V}) - g_i s_{\max} Q_i(M, M)(\bar{V} - V^i)$$
$$\equiv Q(M).$$

The function $Q(M)$ is identical in shape to that in Figure 9, and V_T/R_m plays the role of θ. We cam rewrite this as

$$g^* = g_e Q_e(M, M) - g_i r Q_i(M, M), \tag{3.11}$$

where g^*, r have the same meanings as above. In the limit as M goes to infinity, we obtain

$$2g^* = g_e - g_i r,$$

so that the minimal value of g_i to obtain a bump is

$$g_i^{M=\infty} = (g_e - 2g^*)/r.$$

Since g^* is typically quite small, the difference between this critical value and the value of inhibition that stops a wave, $g_i^{v=0}$, is very small. Nevertheless, the integrate-and-fire calculations suggest that it may be possible to obtain coexistence of localized structures and traveling fronts. In the biophysical model, the threshold for obtaining fronts is very small, so that it would be hard in practice to find this region. However, by injecting a constant hyperpolarizing current into the biophysical model, it may be possible to find both types of behavior.

Remarks.

1. That the width of the bumps tends to infinity as the inhibition decreases is a consequence of assuming that the interaction functions, $J_{e,i}$, have infinite support. If they have a finite extent, then $Q_\alpha(M, M)$ reaches its maximum value of $1/2$ at a finite value of M. Furthermore, bumps that are separated by a distance exceeding the inhibitory extent do not interact, so that it is possible to put many bumps in a given domain.
2. We can get some handle on the dependence of the width on the relative extent of the inhibition to the excitation. Suppose that $J_\alpha(x) = \exp(-|x|/\sigma_\alpha)/(2\sigma_\alpha)$ for $\alpha = e, i$. Then $Q_\alpha(M, M) = [1 - \exp(-M/\sigma_\alpha)]/2$. Let $p = \sigma_i/\sigma_e$. Then equation 3.11 can be rewritten as

$$h(x) = bx - x^p = b + 2c - 1,$$

where $x = \exp(-M/\sigma_i)$, $c = g^*/g_e$ and $b = g_i r/g_e$. We require that $0 < x < 1$ and note that $b + 2x > 1$ since we assume that g_i is larger than $g_i^{M=\infty}$. The function $h(x)$ has roots at, $x = 0$ and $x = b^{1/(p-1)}$. This gives a lower bound to the width of the bump of

$$M_{\min} = \frac{\sigma_i}{\sigma_i/\sigma_e - 1} \ln \frac{g_e}{r g_i}.$$

For $\sigma_i \gg \sigma_e$, the minimum width is proportional to σ_e.

4 Discussion

One of the major classes of excitatory synaptic receptor is the NMDA receptor. It has two defining characteristics: its activation requires that the postsynaptic neuron be active, and it has a long decay time. In this article, we have ignored the voltage dependence of the receptor. This is justified within the active regions since the postsynaptic neuron is firing. Alternatively, we point out that in low magnesium medium, there is no voltage dependence. Indeed, the experiments in Wu and Guan (1999) were in low magnesium. The main property we exploited here was the slow decay of the synapses. The slow decay allows neurons to maintain an active state and thus produce a variety of dynamical patterns. We showed that slow synapses make single self-coupled neurons bistable. Furthermore, when excitable cells are coupled together, the persistent excitation transforms them into oscillators, and the slow decay forces them to oscillate asynchronously. In networks of neurons, the slow decay enables patterns of activity that include propagating wave fronts and localized stationary patterns. Our analysis lumps the inhibitory neurons into the excitatory pool. Thus, one question is whether this makes it more difficult to produce spatial patterns of persistent activity. Wang's recent models (2001) indicate that it is still possible to obtain localized activity even when there is a separate population of inhibitory neurons. In Golomb and Ermentrout (2001), we show that single-spike traveling waves are still possible when there are inhibitory neurons. Similarly, Hansel and Mato (2001) show that persistent activity is also possible in such networks as long as the neurons remain asynchronous. However, inhibition is known to be synchronizing (Ermentrout et al., 2001; Kopell, Ermentrout, Whittington, & Traub, 2000; Ermentrout & Kopell, 1998) when involved in excitatory networks. Thus, there is a danger that the fronts and bumps constructed here can lose stability due to increased temporal correlations in the spikes. This type of instability was described in Bressloff and Coombes (2000) for integrate-and-fire models and more recently in Hansel and Mato (2001) for neurons near a saddle-node bifurcation. Laing and Chow (2001) describe a destabilization of the persistent state as the time constant of the excitatory coupling decreases, leading to synchrony within the bump and then its disappearance. However, for slow enough decay of the synapses, persistence is possible to maintain even if all the neurons are synchronous,

as we showed in section 2. Spike-frequency adaptation through intrinsic potassium currents or indirectly through synaptic depression is a more difficult problem in that it can overcome the long-lasting decay of the excitatory synapses due to its own long-lasting effects. In Pinto and Ermentrout (2001b), we exploited this to produce traveling pulses of activity instead of fronts, and in van Vreeswijk and Hansel (2001), they produce bursting oscillations.

Laing and Chow (2001) found that the bumps that they constructed using the integrate-and-fire model were quite susceptible to noise and thus moved around quite a bit. This appears to be due to the irregular firing at low rates at the edge of the bumps. Thus, at the edges, small amounts of noise can cause the slow-firing neurons to drop out of the bump. This reduces the inhibition and allows previously silent cells to be recruited so that the bump will move in a random fashion. Camperi and Wang (1998) felt that this was a sufficiently difficult problem that they suggested that making individual neurons bistable would help stabilize the bump. Slowly decaying synapses appear to prevent wandering of the bump and encourage stabilization. As we saw in section 2, slowly decaying synapses act to make individual self-coupled neurons bistable, so this could explain the robustness to noise. Simulations of bumps with noise (not shown) indicate that the bumps are quite stable until a critical level of noise is reached. At this point, the noise is sufficient to cause extraneous bumps to appear in the medium, so that rather than a single wandering bump, the medium breaks into multiple bumps. This is possibly due to a so-called Turing instability induced by the noise. That is, the noise allows the neurons to fire in a subthreshold regime, and the lateral inhibition leads to a destabilization of this low (but nonzero) firing rate.

We found that wave fronts can go to zero velocity as the inhibition increases. This contrasts with the case of single spike waves (Golomb & Ermentrout, 2001) where there is a nonzero minimal velocity. The reason is that there are slow and fast velocities for traveling pulses but only fast waves for traveling fronts. The zero velocity we find here is likely to be due to the assumption that the synaptic profile, $s(x, t)$, is monotone in t. However, as the velocity gets sufficiently slow, the synapses should have time to decay enough that this monotone assumption is no longer valid. Thus, in reality, we expect that there will be a limiting velocity whose value depends on the decay rate of the synapses. Indeed, this was shown for single-spike waves in Golomb and Ermentrout (2001).

Appendix: The Biophysical Model

We use a model based on fast currents found in hippocampal neurons (Traub & Miles, 1991). The equations are

$$C\frac{dV}{dt} = I - g_L(V - V_L) - g_K n^4(V - V_K) - g_{Na} m^3 h(V - V_{Na}) - I_{syn},$$

where

$$I_{syn} = g_{syn} s(V - V_{syn}).$$

When there is a network, the synaptic current is the sum of many similar terms (the details are in the main text). Each of the variables, n, m, h, s satisfies equations of the form

$$\frac{dx}{dt} = a_x(V)(1 - x) - b_x(V)x.$$

In our model, $a_m(v) = .32(54 + v)/(1 - \exp(-(v + 54)/4))$, $b_m(v) = .28(v + 27)/(\exp((v + 27)/5) - 1)$, $a_h(v) = .128\exp(-(50 + v)/18)$, $b_h(v) = 4/(1 + \exp(-(v + 27)/5))$, $a_n(v) = .032(v + 52)/(1 - \exp(-(v + 52)/5))$, $b_n(v) = .5\exp(-(57+v)/40)$, and $a_s(v) = 4/(1+\exp(-v/5)$, $b_s = 1/\tau$. The parameters are $g_L = 0.2$, $V_L = -67$, $g_{Na} = 100$, $V_{Na} = 50$, $g_K = 80$, and $V_K = -100$. Typically, we vary g_{syn} and τ. All potentials are in millivolts, conductances are in mS/cm^2 , current in $\mu A/\text{cm}^2$, and $C = 1\mu F/\text{cm}^2$. All equations were solved using XPPAUT (Ermentrout, 2002). The equation files are available upon request.

Acknowledgments

Thanks to Jon Rubin and Carson Chow for a critical reading as well as an anonymous referee for his useful point about the asymptotics in section 2. This research was supported in part by NIMH and NSF.

References

Amari, S. (1977). Dynamics of pattern formation in lateral-inhibition type neural fields. *Biol. Cybernet., 27*, 77–87.

Booth, V., & Rinzel, J. (1995). A minimal, compartmental model for a dendritic origin of bistability of motoneuron firing patterns. *J. Comput. Neurosci., 2*, 299–312.

Bressloff, P. C., & Coombes, S. (2000). Dynamical theory of spike train dynamics in networks of integrate-and-fire oscillators. *SIAM J. Appl. Math., 60*, 828–841.

Camperi, M., & Wang, X. J. (1998). A model of visuospatial short-term memory in prefrontal cortex: Recurrent network and cellular bistability. *J. Computat. Neuroscience, 5*, 383–405.

Chen, Z. Ermentrout, B., & Wang X. J. (1998). Wave propagation mediated by GABAB synapse and rebound excitation in an inhibitory network: A reduced model approach. *J. Comput. Neurosci., 5*, 53–69.

Compte, A., Brunel, N., Goldman-Rakic, P. S., & Wang, X. J. (2000). Synaptic mechanisms and network dynamics underlying spatial working memory in a cortical network model. *Cerebral Cortex, 10*, 910–923.

Destexhe, A., Mainen, Z. F., & Sejnowski, T. J. (1994). Synthesis of models for excitable membranes, synaptic transmission and neuromodulation using a common kinetic formalism. *J. Comput. Neurosci., 3*, 195–230.

Doedel, E. (1981). AUTO: A program for the automatic bifurcation analysis of autonomous systems. *Cong. Num., 30*, 265–284.

Ermentrout, B. (1994). Reduction of conductance based models with slow synapses to neural nets. *Neural Computation, 6*, 679–695.

Ermentrout, B. (1996). Type I membranes, phase resetting curves, and synchrony. *Neural Computation, 8*, 979–1001.

Ermentrout B. (1998a). Linearization of F-I curves by adaptation. *Neural Computation, 10*, 1721–1729.

Ermentrout, B. (1998b). The analysis of synaptically generated traveling waves. *J. Comput. Neurosci., 5*, 191–208.

Ermentrout, B. (2002). *Simulating, analyzing, and animating dynamical systems: A guide to XPPAUT for researchers and students*. Philadelphia: SIAM.

Ermentrout, G. B., & Kopell, N. (1986). Parabolic bursting in an excitable system coupled with a slow oscillation. *SIAM J. Appl. Math., 46*, 233–253.

Ermentrout, G. B., & Kopell, N. (1998). Fine structure of neural spiking and synchronization in the presence of conduction delays. *PNAS, 95*(3), 1259–1264.

Ermentrout, B., Pascal, M., & Gutkin, B. (2001). The effects of spike frequency adaptation and negative feedback on the synchronization of neural oscillators. *Neural Computation, 13*, 1285–1310.

Frankel, P., & Kiemel, T. (1993). Relative phase-behavior of two slowly coupled oscillators. *SIAM J. Appl. Math., 53*, 1436–1446.

Fuster, J. M. (1973). Unit activity in the prefrontal cortex during delayed response performance: neuronal correlates of transient memory. *J. Neurophysiol., 36*, 61–78.

Goldman-Rakic, P. S. (1987). Circuitry of primate prefrontal cortex and the regulation of behavior by representational memory. In F. Blum & V. Mountcastle (Eds.), *Handbook of physiology, vol. 5: The nervous system* (pp. 373–417). Bethesda, MD: American Physiological Society.

Golomb, D., & Amitai, Y. (1997). Propagating neuronal discharges in neocortical slices: Computational and experimental study. *J. Neurophysiol., 78*, 1199–1211.

Golomb D., & Ermentrout, G. B. (2001). Bistability in pulse propagation in networks of excitatory and inhibitory populations. *Phys. Rev. Letters, 86*(18), 4179–4182.

Golomb, D., & Rinzel, J. (1993). Dynamics of globally coupled inhibitory neurons with heterogeneity. *Phys. Rev. E, 48*, 4810–4814.

Gutkin, B. S., Laing, C. R., Colby, C. L., Chow, C. C., & Ermentrout, G. B. (2001). Turning on and off with excitation: The role of spike-timing asynchrony and synchrony in sustained neural activity. *J. Comput. Neurosci., 11*(2), 121–134.

Hansel, D., & Mato, G. (2001). Existence and stability of persistent states in large neuronal networks. *Phys. Rev. Lett., 86*, 4175–4178.

Hansel, D., Mato, G., & Meunier, C. (1995). Synchrony in excitatory neural networks. *Neural Comput., 7*, 307–337.

Hoppensteadt, F., & Izhikevich, E. (1997). *Weakly connected neural nets*. Berlin: Springer-Verlag.

Izhikevich, E. M. (1999). Class 1 neural excitability, conventional synapses, weakly connected networks, and mathematical foundations of pulse-coupled models. *IEEE Trans. Neur. Networks, 10,* 499–507.

Izhikevich, E. M., & Hoppensteadt, F. C. (in press). Slowly coupled oscillators: Phase dynamics and synchronization. *SIAM Journal on Applied Mathematics.*

Kishimoto, K., & Amari, S. (1979). Existence and stability of local excitations in homogeneous neural fields. *J. Math. Biology, 7,* 303–318.

Kopell, N., Ermentrout, G. B., Whittington, M. A., & Traub, R. D. (2000). Gamma rhythms and beta rhythms have different synchronization properties. *PNAS USA, 97,* 1867–1872.

Laing, C. R., & Chow, C. C. (2001). Stationary bumps in networks of spiking neurons. *Neural Comput., 13,* 1473–1494.

Lisman, J. E., Fellous, J.-M., Wang, X.-J. (1998). A role for NMDA-receptor channels in working memory. *Nat. Neurosci., 1,* 273–275.

Netoff, T. I., & Schiff, S. J. (2002). Decreased neuronal synchronization during experimental seizures. *J. Neurosci., 22*(16), 7297–7307.

Osan, R. Curtu, R., Rubin, J., & Ermentrout, B. (in press). Multiple spike waves in integrate and fire neurons. *J. Math. Biology.*

Osan, R., Rubin, J., Curtu, R., & Ermentrout, B. (in press). Traveling waves in a one-dimensional integrate-and-fire neural network with finite support connectivity. *Neurocomputing.*

Pinto, D. J., & Ermentrout, G. B. (2001a). Spatially structured activity in synaptically coupled neuronal networks: II. Lateral inhibition and standing pulses. *SIAM J. Appl. Math., 62*(1), 226–243.

Pinto, D. J., & Ermentrout, G. B. (2001b). Spatially structured activity in synaptically coupled neuronal networks: I. Traveling fronts and pulses. *SIAM J. Appl. Math., 62*(1), 206–225.

Rinzel, J. M., & Ermentrout, G. B. (1998). Analysis of neuronal excitability. In C. Koch & I. Segev (Eds.), *Methods in neuronal modeling* (2nd ed.). Cambridge, MA: MIT Press.

Rubin, J., Terman, D., & Chow, C. (2001). Localized bumps of activity sustained by inhibition in a two-layer thalamic network. *J. Comp. Neurosci., 10,* 313–331.

Sanchez-Vives, M. V., & McCormick, D. A. (2000). Cellular and network mechanisms of rhythmic recurrent activity in neocortex. *Nat. Neurosci., 3,* 1027–1034.

Traub, R. D., & Miles, R. (1991). *Neuronal networks of the hippocampus.* Cambridge: Cambridge University Press.

van Vreeswijk, C., & Hansel, D. (2001). Patterns of synchrony in neural networks with spike adaptation. *Neural Comput., 13,* 959–992.

Wang, X.-J. (1999a). Synaptic basis of cortical persistent activity: The importance of NMDA receptors to working memory. *J. Neurosci., 19,* 9587–9603.

Wang, X.-J. (2001). Synaptic reverberation underlying mnemonic persistent activity. *Trends in Neurosci., 24,* 455–463.

Wu, J. Y., & Guan, L. (1999). Spatio-temporal patterns of network co-activation in adult neocortical slices. *Soc. Neurosci. Abs., 25,* 404.

Wu, J. Y., Guan, L., & Tsau, Y. (1999). Propagating activation during oscillations and evoked responses in neocortical slices. *J. Neurosci., 19,* 5005–5015.

Received March 7, 2003; accepted May 1, 2003.